Coastal Dynamics 2017
Paper No. 258

THE EFFECT OF ISLAND SLOPES ON WAVE TRANSFORMATION DURING OVERWASH AND INUNDATION

Anita Engelstad[1], Gerben Ruessink[1], and Maarten van der Vegt[1]

Abstract

Overwash and inundation of barrier islands can lead to vertical accretion of sediment; however, the hydrodynamic processes during these floodings need to be investigated in more detail. The non-hydrostatic wave-flow model SWASH is used to investigate the effect of beach slope steepness on sea-swell and infragravity wave heights and wave shape during inundation. The model-field data comparison shows satisfying results for sea-swell waves, but overestimates infragravity waves and wave asymmetries and skewness, which is most likely caused by the use of the 1-d profile mode. The comparison of different beach slopes suggests that for a steep beach slope less energy is dissipated before the crest compared to gentler slopes, but this is compensated by higher dissipation onshore of the crest. Wave asymmetries suggest that the dissipation of sea-swell waves as well as infragravity waves is primarily caused by wave breaking.

Key words: hydrodynamics, overwash, inundation, wave heights, wave shape, sediment transport, numerical modelling, barrier islands

1. Introduction

The growth of barrier islands is important for their survival in times of sea level rise. Overwash and inundation of barrier islands are natural processes, which can transport sediment onshore (Leatherman, 1975; Sallenger, 2000) and increase the resilience of barrier islands due to sediment accretion. Overwash is the process during which water, carrying suspended sediments, overtops the beach- or dune crest without directly returning to the sea (Donelly et al., 2006), while during inundation the area is continuously submerged (Sallenger, 2000). These events might cause island instabilities (Donelly et al., 2006; Safak et al., 2016), such as the breaching or the landward transition of islands (roll-over), but they can also lead to vertical accretion.
Overwash and inundation are storm-driven events, which makes the observation of hydrodynamics difficult. As a result, not much about the hydrodynamic processes during flooding is known. So far, most studies on overwash and inundation focus on morphological changes before and after storms (Morton and Sallenger, 2003; Nielsen and Nielsen, 2006; Matias et al., 2008), laboratory work (Edge et al., 2007; Matias et al., 2013), and numerical modeling (Van Dongeren and Van Ormondt, 2007; Mc-Call et al., 2010, 2011). Some studies include onsite hydrodynamic measurements (Fisher et al. , 1974; Leatherman , 1976; Holland et al., 1991; Hoekstra et al., 2009; Matias et al., 2010; Van der Vegt and Hoekstra, 2012; Sherwood et al., 2014; Engelstad et al., 2017).

Local characteristics, such as the size and alignment of the back barrier area and the geometry of the island, can affect the hydrodynamics during inundation. Observational studies (Sherwood et al., 2014; Safak et al., 2016; Engelstad, et al., 2017) have found that increased water levels in the back barrier basin can be important drivers of flow velocities, which might even reverse the flow direction to an offshore flow. In addition, cross-shore velocities can be quite strong compared to velocities on a closed-beach-dune system. Further, during the inundation of a low lying, gently sloping barrier island tail, infragravity (0.005-0.05 Hz)

[1]Department of Physical Geography, Faculty of Geosciences, Utrecht University, P.O. Box 80.115, 3508 TC Utrecht, the Netherlands. A.C.Engelstad@uu.nl

and sea-swell waves (0.05-1 Hz) were observed (Engelstad et al., 2017) to preserve part of the energy onshore of the beach crest (highest point in the profile). Here, infragravity waves were found to be onshore progressive which is consistent with findings on gentle sloping, closed beaches (De Bakker et al.,2014; van Dongeren et al.,2007). The main dissipation mechanism for infragravity and sea-swell waves was identified to be wave breaking which, again, is in agreement with observations on gentle sloping beaches (Van Dongeren et al., 2007; De Bakker et al., 2014, 2015).
However, is not known if and how the beach steepness influences the wave transformation and wave shape on the beach slope and onshore of the beach crest during inundation. Generally, before the onset of wave breaking, waves propagate from the deep water, offshore region into the nearshore region where they start to shoal due to the decrease in water depth. During this process, they transform from a sinusoidal to a skewed shape with broad, shallow troughs and narrow, steep crests. In addition, the wave shape changes further into an asymmetric shape at the onset of wave breaking with forward leaning waves that have a steep wave front and a more gentle back. Asymmetry and skewness influence sediment stirring and transport (e.g. Ruessink et al., 2011; Fernàndez-Mora, 2015), and while sediment transport under asymmetric waves is onshore directed, transport can be onshore or offshore directed under skewed waves. The offshore transport is due to a phase lag, which stirs the sediment under the crest and transports it offshore under the trough (e.g., Hoefel and Elgar, 2003; Grasso et al., 2011).

The motivation for this study is that at the moment the restoration of overwash and inundation processes on barrier islands in the Netherlands is considered. Most barrier islands in the Netherlands are heavily protected against storms by natural dunes and artificial sand drift dikes, which are cutting off the distribution of sediment to areas landward of the protection. Restoration would involve the re-opening of some of the dikes and dunes in uninhabited areas. However, to evaluate the feasibility of restoring these natural processes, and to be able to determine design criteria for openings, the effect of regional aspects such as the steepness of the beach slope on wave processes during inundation need to be known.
Here, we investigate the question of how the beach steepness influences infragravity and sea-swell wave heights and the deformation of waves on the beach slope and on the island flat landward of the crest. Further, the influence of these parameters on the cross-shore flow will be examined. For this, we use the numerical model SWASH (Zijlema et al., 2011), which is introduced in Section 2. Results for a model validation with field observations and results for a comparison of beach slopes with varying steepness are shown in Section 3, followed by some remarks about future work in Section 4. Finally, the results are summarized in Section 5.

2. Methods

To simulate the transformation of infragravity (~0.005-0.05 Hz) and sea-swell (~0.05-1 Hz) waves on varying beach slopes during inundation, the non-hydrostatic wave-flow model SWASH (Zijlema et al., 2011) was used to investigate intra-wave properties. SWASH (Simulating WAves till SHore) is based on the nonlinear shallow water equations, which describe the conservation of mass and momentum, and accounts for non-hydrostatic pressure. For a full model description see Zijlema et al. (2011).
To avoid wave reflection at the basin side, a 500 m sponge layer was used together with a radiation condition, which only allows for outgoing waves. At the sea side boundary, the boundary type was chosen to be weakly reflective.
The vertical resolution was set to 2 vertical layers, while the horizontal resolution was set to 0.2 m. The stability of the computations is assured by setting the time-step, based on the Courant number, to 0.0125 s for all runs. Dissipation by wave breaking is captured following the approach by Smit et al, 2013. To account for dissipation by bottom friction, the Manning's roughness coefficient was set to 0.019. Wind forcing and atmospheric pressure is ignored to simplify the computations. Simulations were run over 4 hours to allow for sufficient spin-up time over the large domain (described below), and bulk parameters were averaged over the last hour. Boundary conditions were implemented with observations (also described below).

The observations used here for the model-data comparison were collected during 11 inundation events on a

barrier island tail in the Netherlands in the winter of 2014/2015 (for details on data collection and analysis see Engelstad et al., 2017). The field area is approximately alongshore uniform, low-lying (the beach crest at the highest point was located at ~1.65 m above mean sea level (MSL)), and vegetation free. The steepest slope (measured with a Real Time Kinematic Global Positioning System, RTK-GPS) was ~ 1/100.
Observations of water levels and waves were collected on an ~ 1.3 km instrument transect, which stretched from the North Sea to the Wadden Sea (the back barrier basin), with 10 pressure sensors (Ocean Sensor System Wave Gauge, type OSSI-010-003C), measuring at 10 Hz. The observations showed that in addition to the waves from the North Sea, waves also entered the field site from the Wadden Sea side. These waves were generated in the Wadden Sea and are not accounted for in the SWASH simulations. Also, due to the storm surge, water levels at the Wadden Sea side were almost always higher after high tide compared to the North Sea side. For the model-data comparison, we use data collected during the 7th flooding (further called F7) one hour before high tide when water levels in the North and Wadden Sea were roughly the equal (1.90 m), and during the 8th flooding (F8) at high tide when the water level was lower in the Wadden Sea compared to the North Sea (1.85 m vs 1.75 m). These floodings were chosen to avoid the influence of higher water levels in the Wadden Sea, since the water level in the model implementation was hold constant. The offshore significant wave height was 3.13 m and 2.96 m with a peak period of 10 s and 8 s during F7 and F8, respectively. Offshore wave conditions were measured by a wave buoy (Schiermonnikoog Noord) and water levels were measured by a tidal station (Huibertgat). For the slope comparisons, the deepest recorded flooding (5.9 m significant wave height, 12 s wave period and a 2.65 m water level) was used as boundary conditions to assure that waves are high enough onshore of the crest to allow for a reliable evaluation of the wave shape. This flooding was not used for the model-data comparison since the water levels were higher on the Wadden Sea side for the entire duration of the inundation. All wave and water level data were averaged over an hour around high tide.

The model design for the model-data comparison, as well as for the inter-slope comparison, is based on the observations. The bottom profile for the model-data comparison (Figure 1a) is a combination of the island profile measured during instrument deployment and offshore measurements made available by Rijkswaterstaat (RWS, Dutch ministry of infrastructure and the environment). In addition, the bed profiles were extended at either side of the transect (Figure 1a, km 0-3 and km 14-17), resulting in a total domain length of ~ 17.5 km, starting in 20 m water depth The bottom profiles for the slope inter-comparisons are a simplified version of the bottom profile used for the model-data comparison. Here, the model was run out of 12 m water depth over a total distance of more than 10 km. For the slope variations only the beach slope was varied (Figure 1b). Since beach slopes in the Netherlands are usually gentle to moderate, we consider here beach slopes of 1/30 (“steep”), 1/70 (“medium”) and 1/120 (“gentle”).

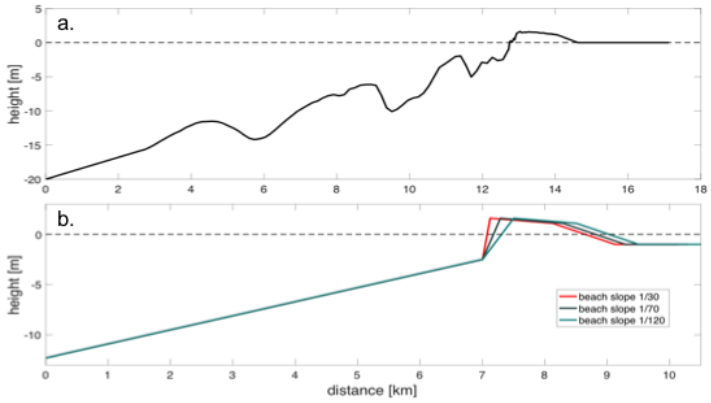

Figure 1. Profile for the model-data comparison (a.) and the simplified slope (b.) with the different beach slopes.

The wave shape is determined by wave skewness and asymmetry. Skewness describes the wave asymmetry in a horizontal plane for waves with long, shallow troughs and high narrow crests, whereas asymmetry describes the asymmetry in a vertical plane with saw-tooth shaped, forward pitched leaning waves. The

increase in skewness and asymmetry is measured by an increase in positive and negative values, respectively, up to maximum values around ±2, while for sinusoidal waves asymmetry and skewness are zero. Asymmetry and skewness are estimated by the normalized third moment of the sea surface following Elgar (1985).

3. Results

3. 1. *Model-data comparison*

To investigate the ability of the SWASH model to hindcast the conditions observed in the field, we compare observed and modeled water levels, cross-shore velocities, infragravity and sea-swell wave heights, as well as infragravity and sea-swell wave skewness and asymmetry.
Overall, the model-field data agreement is satisfactory. The wave set-up at the North Sea side is slightly overestimated (Figure 2a) by roughly 0.13 m and 0.05 m for F7 and F8, respectively. At the Wadden Sea side, the water level during F7 is overestimated by 0.04 m while it is underestimated during F8 which could be caused by a locally already high water level in the Wadden Sea. The observed higher water level on the Wadden Sea side causes a gentler surface elevation slope from the beach plain to the Wadden Sea than predicted, resulting in lower than modeled velocities (Figure 2c). The velocity overestimation for F7, is also most likely caused by the steepness of the surface elevation slope, since the surface elevation at the crest is more overestimated at the Wadden Sea.

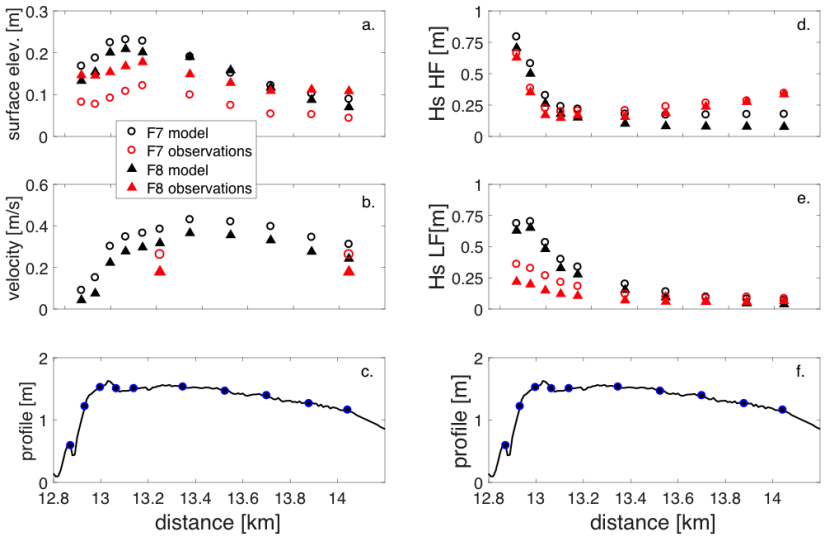

Figure 2. Model results for sea surface elevation (a.), velocity (b.), sea-swell (HF, d.) and infragravity (LF,e.) wave heights. Instrument locations (blue dots in c. and f.) are shown on the island profile. The North Sea is to the left, the Wadden Sea is to the right.

While predicted sea-swell wave heights show relatively good agreement (Figure 2d.) on the North Sea side (albeit some overestimation can be noted) and the center of the instrument transect, they are increasingly under-predicted towards the Wadden Sea. This is to be expected since waves, generated in the Wadden Sea, were observed to propagate offshore during inundation. This, as mentioned before, was ignored in the model implementations. The slight over-prediction at the other locations is likely a result of the higher modeled than observed water levels.
Infragravity wave heights, on the other hand, are consistently overestimated (Figure 2e.) on the North Sea side by roughly a factor of 2. The overestimation of infragravity wave energy by SWASH was also observed by de Bakker et al. (2014). The authors attributed this to the fact that directional spreading cannot

be included in profile mode in SWASH, leading to the overestimations. Indeed, better agreements between model and field observations for infragravity wave energy were found using 2-D simulations (Rijnsdorp et al., 2014), although infragravity waves were still slightly overestimated.
To avoid the influence of waves from the Wadden Sea on asymmetry and skewness results, sea-swell asymmetry and skewness were only considered in the frequency range 0.05-0.3 Hz and cut-off for wave heights smaller than 0.2 m. The comparison of predicted and observed high frequency asymmetry (Figure 3 a. and c.) shows good agreement for the first two locations on the beach slope, but an overestimation on the crest and on the flat. The comparison gets better again on the Wadden Sea side (shown only for F7). High frequency skewness also shows good agreement on the Wadden Sea side, while it is over-predicted on the North Sea side and most of the flat. The agreement is much better for asymmetry and skewness in the infragravity range for F7 (Figure 3b.) with the exception of the overestimation of asymmetries toward the Wadden Sea. On the other hand, infragravity skewness and asymmetry for F8 (Figure 3d.) show the same overestimation as can be seen for the sea-swell range.
The overestimations of wave asymmetry and skewness could at least partly be the result of the infragravity wave height overestimation in the 1-D simulations and the merging of waves (Tissier et al., 2015). Depth modulation by infragravity waves (causing higher local water depths under the crest as under the trough) allows high-frequency waves with higher amplitudes to ride on the crest of the infragravity waves while they are lower on the trough of the infragravity wave (Figure 4).

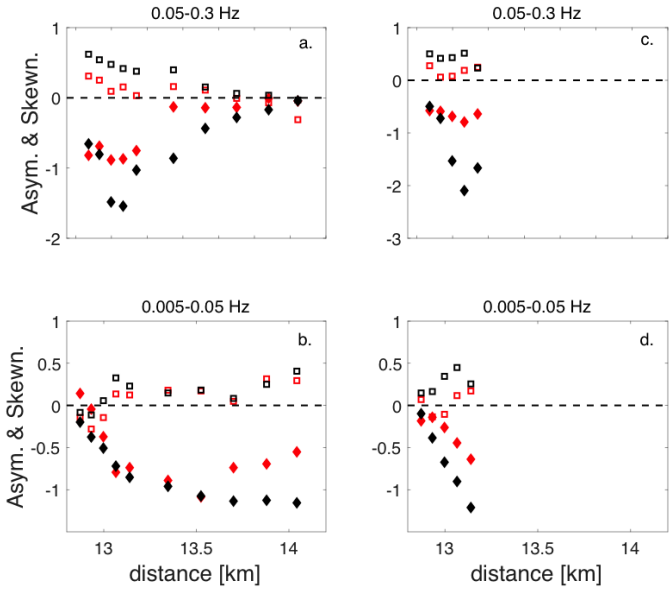

Figure 3. Observations (red) and model results (black) for sea-swell (a. and c.) and infragravity (b. and d.) asymmetries (diamonds) and skewness (squares) for F7 (a. and b.) and F8 (c. and d.). For instrument locations refer to Figure 2. F8 asymmetry and skewness are only shown for the first five locations due to small wave heights. The North Sea is to the left, the Wadden Sea is to the right.

While SWASH overestimates the skewness and asymmetry when compared to our field data, the general trends, which are visible in the field data, are captured fairly well. For laboratory data (1D), Smit et al. (2014) found good model-data agreement for wave skewness and asymmetry, as were found for (infragravity) wave heights and other wave parameters (Rijnsdorp et al., 2012; Zijlema et al. 2011; Zijlema, 2012). This suggests that while computations in 1-D mode offer only partly satisfactory results for the field data comparison, it is sufficient for a comparison of waves transformation and cross-shore currents over various beach slopes, especially since the use of a 2-D grid is computational very expensive.

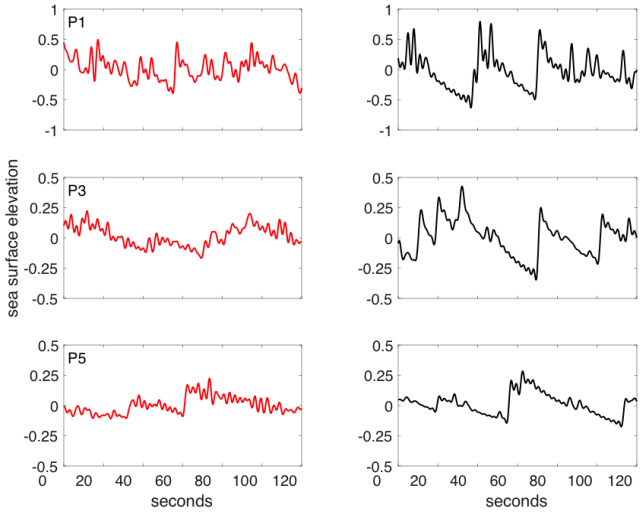

Figure 4. Observed (left panels) and modeled (right panels) sea surface elevations for F7. Sea surface elevations were filtered (0.005-0.3 Hz) to exclude locally generated wind waves. Shown are two locations on the slope (P1 and P3) and one after the crest (P5).

3. 2. *Slope comparisons*

To investigate the effect of the beach slope steepness, the model was run over 3 different slopes, described in Section 2.2. The results suggest that sea-swell waves are higher at the beach crest for a steep slope compared to gentler slopes (see intersect of dashed line with solid line in Figure 5). For a gentle slope, most of the energy in the sea-swell range is dissipated before the wave crest, while for a steep slope dissipation continues onshore of the crest until wave heights are the same as for the gentler slopes.

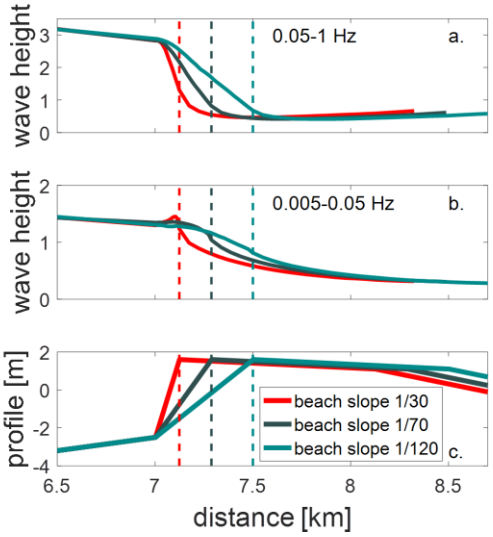

Figure 5. HF (a.) and LF (b.) predictions of wave heights for three different profiles (c.). The vertical dashed lines show the locations of the beach crests.

On the flat, onshore of the crest, waves don't lose their energy entirely and wave heights even increase again slightly, which might be a result of our fixed cut-off between infragravity and sea-swell waves. For a steep slope, higher waves at the beach crest are also found for infragravity waves (Figure 5b). However, at the onset of the slope, infragravity wave heights increase for a steep slope, but start to decrease again just before the crest. The increase in infragravity wave heights on the slope might be caused by wave reflection (De Bakker et al., 2016). Onshore of the crest, infragravity waves continue to loose energy across the flat. Generally, the results show that more wave energy across the spectrum is conserved until after the crest for a steep slope where strong dissipation of wave energy continues.

The comparison of surface elevations for the different beach slopes show higher surface elevations for the steep slope.. The variations in surface elevation (Figure 6a) are caused by wave set-up due to wave breaking. Since waves for the steep slope continue to break after the crest, this location is situated well onshore of the crest. Further, since set-up is both a function of the radiation stress caused by wave breaking and the water depth, this results in a higher surface elevation for the steep slope where breaking continues on the flat in lower water depths. The surface elevation for all slopes returns to about the same level since they are forced by the boundary conditions. The cross-shore velocity (Figure 6b) is highest for the steep slope, suggesting that the velocity after the crest is mostly driven by the pressure gradient.

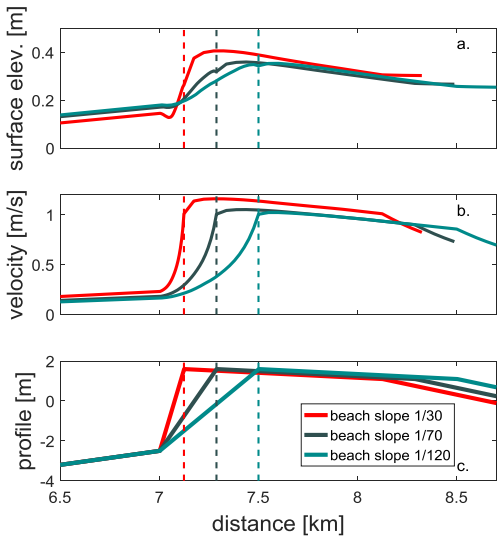

Figure 6. Surface elevation (a.) and cross-shore velocity (b.) predictions for three different profiles (c.). The vertical dashed lines show the locations of the beach crests.

As mentioned in Section 2.1., the wave shape is determined by wave asymmetry and skewness. Wave skewness in the sea-swell range is already high when waves reach the beach slope (Figure 7a), due to the decrease in water depth on the offshore slope (Figure 1b). The skewness decreases significantly around the crest for the steep slope, probably due to higher dissipation rates, but increases again slightly after wave dissipation ends. However, it remains lower than for the gentler slopes. Wave asymmetries develop from the onset of the beach slopes for all cases (Figure 7a) and are slightly higher for the steep slope after the crest, indicating continued wave breaking after the highest point in the profile. Further onshore, asymmetries decrease, suggesting that sea-swell wave breaking stopped.
Skewness and asymmetry of infragravity waves increase noticeable only onshore of the crest (Figure 7b) for the steep and gentle slopes. However, they begin to increase before the crest for the gentle slope. Generally, the increase in infragravity asymmetry and skewness is most likely caused by the release of bound waves on the slope during wave breaking, after which they continue to propagate onshore as free waves. These waves continue to deform in the shallow water onshore of the crest.
Further, wave asymmetry and skewness values for the infragravity range are somewhat lower than for the

sea-swell waves, suggesting that the ratio of high peaks compared to long shallow troughs is lower and infragravity waves are less pitched forward. However, the continued decrease in infragravity wave heights and high asymmetry values suggests that these waves are breaking.

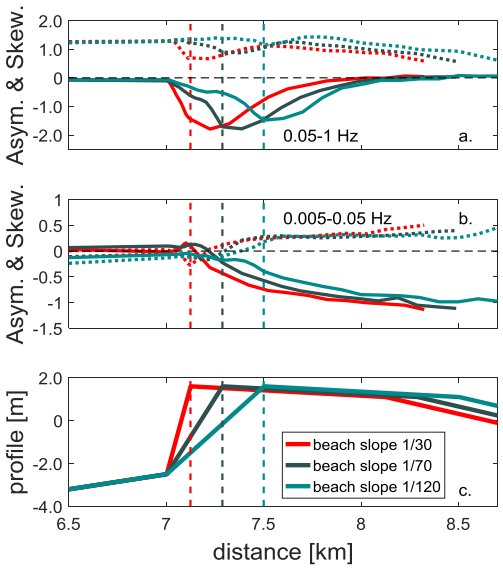

Figure 7. HF (a.) and LF (b.) predictions of wave asymmetry (solid lines) and skewness (dotted lines). The vertical dashed lines show the locations of the beach crests.

4. Future work

The model-data comparison showed satisfying results for sea-swell wave heights, while infragravity waves were over-estimated, as were (high-frequency) wave skewness and asymmetry. Since this is most certainly caused by our 1-D approach, we will evaluate infragravity waves, wave asymmetry and skewness further with a 2-D model. Additionally, we will investigate the contribution of currents, wave asymmetry and skewness on sediment transport on the beach slope and the flat.
The underlying mechanism, which causes sea-swell wave asymmetries to cease on the slope while waves continue to be skewed as seen in Section 3, will also be further investigated.

5. Conclusions

The model-field data comparison showed satisfying results for sea-swell wave height, while SWASH over-predicted infragravity waves by a factor of ~ 2 at the North Sea side. This is to be expected since the 1-D, profile mode cannot account for directional wave spreading. The 1-D approach also shows limitation when comparing field data with modeled wave asymmetries and skewness, which are mostly overestimated. However, the model captured the spatial trends well.
The modeled comparison of different beach slopes suggests that the steepness of the slope not only influences wave and current dynamics on the slope, but also onshore of the crest. Generally, more infragravity and sea-swell wave energy is dissipated on a gentle slope compared to a steep slope, which is in agreement with findings on closed beaches. Consequently, the higher waves on the beach crest for the steep slope lead to more dissipation onshore of the crest compared to the gentler slopes. The asymmetric, forward leaning shape of the waves develops for all slopes with the onset of the beach slope, and continues onshore of the crest, suggesting that the dissipation of sea-swell and infragravity waves is (mostly) due to wave breaking. Shoaling and breaking of infragravity waves only starts after the breaking of the sea-swell waves has started on the beach slope, which causes the releases of the bound infragravity waves. Velocities

onshore of the crest are higher for the steep slope, which is caused by a higher wave set-up due to wave breaking. The importance of the various processes for sediment transport needs to be investigated further.

Acknowledgements

We thank Pieter Smit for recommendations on the SWASH implementations. This work is supported by the Netherlands Organisation for Scientific Research (NOW), as well as by Natuurmonumenten, the National Forest Service (Staatsbosbeheer, SBB), and the Wadden Academy.

References

De Bakker, A. T. M., M. F. S. Tissier, and B. G. Ruessink, 2014. Shoreline dissipation of infragravity waves. *Continental Shelf Res*earch, 72, 73–82, doi: 10.1016/j.csr.2013.11.013.

De Bakker, A. T. M., M. F. S. Tissier, and B. G. Ruessink, 2016. Beach steepness effects on nonlinear infragravity-wave interactions: A numerical study. *Journal of Geophysical Research: Oceans*, 121, 554–570, doi:10.1002/2015JC011268.

Donnelly, C., N. Kraus, and M. Larson, 2006. State of knowledge on measurement and modeling of coastal overwash. *Journal of Coastal Research*, 965-619991, doi:10.2112/04-0431.1.

Edge, B. L., Y. H. Park, and M. Overton, 2007. Experimental study of overwash, in *Proceedings Coastal Sediments*, vol. 7, pp. 2074–2083, doi:10.1061/40926(239)163.

Elgar, Steve, 1987. Relationships involving third moments and bispectra of a harmonic process. *IEEE transactions on acoustics, speech, and signal processing* 35.12: 1725-1726.

Engelstad, A., B.G. Ruessink, D. Wesselman, P. Hoekstra, A. Oost, and M. van der Vegt, 2017. Observations of waves and currents during barrier island inundation, *Journal of Geophysical Research: Oceans*, 122, doi:10.1002/2016JC012545.

Fernández- Mora, A., Calvete, D., Falqués, A., & Swart, H. E. ,2015. Onshore sandbar migration in the surf zone: New insights into the wave- induced sediment transport mechanisms. *Geophysical research letters*, *42*(8), 2869-2877.

Fisher, J. S., S. P. Leatherman, and F. C. Perry, 1974. Overwash processes on Assateague Island, in *Proceedings of 14th Conference on Coastal Engineering*, pp. 1194–1211, ASCE, Copenhagen, Denmark, doi:10.1061/9780872621138.073.

Grasso, Florent, Hervé Michallet, and Eric Barthelemy, 2011. Sediment transport associated with morphological beach changes forced by irregular asymmetric, skewed waves. *Journal of Geophysical Research: Oceans* 116.C3.

Hoefel, Fernanda, and Steve Elgar, 2003. Wave-induced sediment transport and sandbar migration. *Science* 299.5614: 1885-1887.

Hoekstra, P., M. ten Haaf, P. Buijs, A. Oost, R. Klein Breteler, K. van der Giessen, and M. van der Vegt, 2009. Washover development on mixed-energy, mesotidal barrier island systems, in *Coastal Dynamics*, vol. 83, pp. 25–32, World Sci.

Holland, K. T., R. A. Holman, and A. H. Sallenger, 1991. Estimation of overwash bore velocities using video techniques, in *Coastal Sediments*, pp. 489–497, ASCE, doi:10.5670/oceanog.1993.02.

Leatherman, S. P., 1976. Barrier island dynamics: Overwash processes and Eolian transport, *Coastal Engineering Proceedings*, 1(15), doi:10.1061/9780872620834.114.

McCall, R. T., J. S. M. Van Thiel De Vries, N. G. Plant, A. R. Van Dongeren, J. A. Roelvink, D. M. Thompson, and A. J. H. M. Reniers, 2010. Two-dimensional time dependent hurricane overwash and erosion modeling at Santa Rosa Island. *Coastal Engineering*, 57(7), 668–683, doi:10.1016/j.coastaleng.2010.02.006.

McCall, R. T., N. Plant, and J. Van Thiel de Vries, 2011. The effect of longshore topographic variation on overwash modeling. *Coastal Engineering Proceedings*, 1(32), 36, doi:10.9753/icce.v32.sediment.36.

Matias, A., O_. Ferreira, A. Vila-Concejo, T. Garcia, and J. A. Dias, 2008. Classification of washover dynamics in barrier islands. *Geomorphology*, 97(3), 655–674, doi:10.1016/j.geomorph.2007.09. 010.

Matias, A., O_. Ferreira, A. Vila-Concejo, B. Morris, and J. A. Dias, 2010. Short-term morphodynamics of non-storm overwash. *Marine Geology,* 274(1), 69–84, doi:10.1016/j.margeo. 2010.03.006.

Matias, A., G. Masselink, A. Kroon, C. E. Blenkinsopp, and I. L. Turner, 2013). Overwash experiment on a sandy barrier. *Journal of Coastal Research*., 1(65), 778, doi:10.2112/si65-132.1.

Morton, R. A., and A. H. Sallenger Jr., 2003. Morphological impacts of extreme storms on sandy beaches and barriers. *Journal of Coastal Research*, 560–573.

Nielsen, N., and J. Nielsen, 2006. Development of a washover fan on a transgressive barrier, Skallingen, Denmark. *Journal of Coastal Research*, 107–111.

Rijnsdorp, D. P., Ruessink, G., and Zijlema, M., 2015. Infragravity-wave dynamics in a barred coastal region, a numerical study. *Journal of Geophysical Research: Oceans*, 120(6), 4068-4089.

Ruessink, B. G., Michallet, H., Abreu, T., Sancho, F., Van der Werf, J. J., & Silva, P. A., 2011. Observations of

velocities, sand concentrations, and fluxes under velocity- asymmetric oscillatory flows. *Journal of Geophysical Research: Oceans*, 116(C3).

Safak, I., J. C. Warner, and J. H. List, 2016. Barrier island breach evolution: Alongshore transport and bay-ocean pressure gradient interactions. *Journal of Geophysical Research: Oceans*, 121, 8720–8730, doi:10.1002/2016JC012029.

Sallenger Jr., A. H., 2000. Storm impact scale for barrier islands. *Journal of Coastal Research*, 890–895, doi:10.1306/44b4ba04-170a-11d7- 8645000102c1865d.

Sherwood, C. R., J. W. Long, P. J. Dickhudt, P. S. Dalyander, D. M. Thompson, and N. G. Plant, 2014. Inundation of a barrier island (Chandeleur Islands, Louisiana, USA) during a hurricane: Observed water-level gradients and modeled seaward sand transport. *Journal of Geophysical Research: Earth Surface*, 119, 1498–1515, doi:10.1002/2013JF003069.

Smit, P., Zijlema, M., & Stelling, G. ,2013. Depth-induced wave breaking in a non-hydrostatic, near-shore wave model. *Coastal Engineering*, *76*, 1-16.

Smit, P., Janssen, T., Holthuijsen, L., & Smith, J.,2014. Non-hydrostatic modeling of surf zone wave dynamics. *Coastal Engineering*, *83*, 36-48.

Tissier, M., Bonneton, P., Michallet, H., & Ruessink, B. G., 2015. Infragravity- wave modulation of short- wave celerity
in the surf zone. *Journal of Geophysical Research: Oceans*, *120*(10), 6799-6814.

Van der Vegt, M., and P. Hoekstra, 2012. Morphodynamics of a storm-dominated, shallow tidal inlet: The Slufter, the Netherlands, *Netherlands Journal of Geoscience*,, 91(3), 325–339, doi:10.1017/s0016774600000470.

Van Dongeren, A., and M. Van Ormondt, 2007. Hydrodynamic aspects of overwash, Framework: H&I Zeereep (Report in Dutch), report Z, 4412, 33, WL Delft Hydraulics.

Van Dongeren, A., J. Battjes, T. Janssen, J. Van Noorloos, K. Steenhauer, G. Steenbergen, and A. J. H. M. Reniers, 2007. Shoaling and shore- line dissipation of low-frequency waves. *Journal of Geophysical Research.*, 112, C02011, doi:10.1029/2006JC003701.

Zijlema, M., Stelling, G., Smit, P., 2011. SWASH: An operational public domain code for simulating wave fields and rapidly varied flows in coastal waters. *Coastal Engineering*, 58 (10), 992-1012.